Application of the Nonlinear SST Turbulence Model for Simulation of Anisotropic Flows

Andrey A. Savelyev[1] (iD)*, Innokentiy A. Kursakov* (iD)*, Evgeniy S. Matyash*[1]*, Evgeny V. Streltsov*[1]*, Ruslan A. Shtin*[1]

The application of the nonlinear SST turbulence model (SST NL) for the calculation of flows with turbulence anisotropy is considered. The results of the following validation test cases are presented: the flow in a square duct, the corner flow separation at a wing-body junction (NASA Juncture Flow) and the transonic wing flow (NASA CRM). The nonlinear model has been found to significantly improve the quality of simulating the anisotropic flows as compared to models based on the Boussinesq hypothesis. It is shown that the model prevents false corner separation at the wing-body junction and thereby achieves a qualitative improvement in simulation results. The test case of the transonic wing flow revealed an upstream displacement of the shock wave on the upper side of the wing which leads to an underestimation of the lift force when using the SST NL model. In all the tests considered, the SST NL model required an increase in computational cost of at most 5 % compared to the conventional SST model.

Keywords: turbulence model, nonlinear SST, SST NL, turbulence anisotropy, corner flow, corner separation.

Introduction

The main tool currently used in studies of aircraft aerodynamics is the numerical solution of the Reynolds-averaged Navier–Stokes equations, closed by a turbulence model. The most common turbulence models are the Spalart–Allmaras (SA) [1, 21], Menter (SST) [11, 12] and their modifications (e.g., [8]). Both models belong to the family of linear turbulent viscosity models (LEVM) based on the Boussinesq hypothesis, which assumes a linear relationship between the Reynolds stress tensor and the mean velocity gradient. This limits their applicability to the situations in which the flow is mainly affected by a single component of the stress tensor. For more complex flows (e.g., corner flows or separation flows), the effects of turbulence anisotropy appear that cannot be described by the Boussinesq hypothesis.

A practically important example of such a flow is the corner flow near the wing-fuselage junction: calculations using Boussinesq models predict extensive corner flow separation, even at small angles of attack. At higher values of lift on transonic regimes the separation starts interacting with the shock wave, which can lead to global changes in the pressure distribution on the upper surface of the wing and, consequently, to a noticeable reduction of the lift force. Such an effect, observed in the computational studies of the models DLR-F6 [14] and CRM [23], is not confirmed by experimental tests.

In order to correctly describe corner flows, it is necessary to use more complex turbulence models that can reproduce the anisotropy of the Reynolds stress tensor. These are primarily differential models for Reynolds stresses (DRSM) [7]. DRSM models require solving a specific transfer equation for each component of the Reynolds stress tensor. This noticeably increases the computational resource requirements, and makes it more difficult to formulate boundary conditions. In addition, the nonlinearity of these models can lead to a lack of numerical stability, especially when dealing with complex flows [4]. For these reasons, the DRSM models are rarely used in practical applications.

---

[1]Central Aerohydrodynamic Institute (TsAGI), Zhukovsky, Russia

Another approach is the EARSM [24] models, which use explicit algebraic relations between the Reynolds stresses and the strain rate tensor. In terms of physical processes simulating, the EARSM models are intermediate between the DRSM and LEVM approaches and can adequately describe some of the physical phenomena beyond the Boussinesq hypothesis.

Non-linear extensions of Boussinesq models (Non-linear Eddy Viscosity Models, NLEVM) can also be referred to as the Reynolds stress models, since their final stress tensor relations have the same form as in EARSM. The most popular in this family is a modification of the Spalart–Allmaras model – SA QCR [20], which uses a quadratic function from the strain rate and vorticity tensors to model the Reynolds stress tensor. This model, although slightly more complicated, allows a better simulation of corner flows. The present work considers a nonlinear modification of the SST turbulence model – the SST NL model proposed by Garbaruk and Matyushenko [9]. To determine the Reynolds stresses, it combines the linear part from the SST model and the nonlinear part from the S BSL EARSM model [10].

The purpose of this paper is to test the SST NL model both on model test cases and on configurations of interest for practical applications. The paper is organized as follows: Section 1 presents the formulation of the SST NL model [9] and a brief description of the EWT-TsAGI program used. Section 2 presents the results of the test calculations: turbulent flow in a square duct, wing-fuselage junction flow separation on the NASA Juncture Flow model [19], transonic wing flow on the NASA CRM model [13]. The conclusions are given in the final section.

1. Methodology

The expression for the Reynolds stresses in the SST model [11] has the following form:

$$\tau_{ij} = \frac{2}{3}k\delta_{ij} - 2\nu_t S_{ij}, \tag{1}$$

where $\nu_t = \dfrac{a_1 k}{\max{(a_1\omega, SF_2)}}$ is the turbulent eddy viscosity, $S = \sqrt{2S_{ij}S_{ij}}$ – strain rate invariant, F_2 – SST blending function, and $a_1 = 0.31$.

The S BSL EARSM model proposed in [10] is a development of the WJ EARSM [24]. The Reynolds stresses are defined using the anisotropy tensor:

$$\tau_{ij} = \frac{2}{3}k\delta_{ij} + ka_{ij}. \tag{2}$$

The anisotropy tensor is expanded in terms of the tensor basis as follows [15]:

$$a_{ij} = \beta_1 T_{1,ij} + \beta_3 T_{3,ij} + \beta_4 T_{4,ij} + \beta_6 T_{6,ij}. \tag{3}$$

According to [10], the tensor basis can be expressed in a modified (compared to [15]) form:

$$T_{1,ij} = S_{ij}^*, \ T_{3,ij} = \Omega_{ik}^*\Omega_{kj}^* - \frac{1}{3}II_\Omega^*\delta_{ij}, \ T_{4,ij} = S_{ik}^*\Omega_{kj}^* - \Omega_{ik}^*S_{kj}^*,$$
$$T_{6,ij} = S_{ik}^*\Omega_{kl}^*\Omega_{lj}^* + \Omega_{ik}^*\Omega_{kl}^*T_{1,ij} - \frac{2}{3}IV^*\delta_{ij} - II_\Omega^*S_{ij}^*. \tag{4}$$

Here $S_{ij}^* = \tau S_{ij}$ and $\Omega_{ij}^* = \tau\Omega_{ij}$ are dimensionless strain and vorticity tensors, and $\tau = \max\left[1/(\beta^*\omega), 6\sqrt{\nu/(\beta^* k\omega)}\right]$ is the turbulent time scale. The coefficients β are expressed through the tensor invariants $II_S^* = S_{mn}^*S_{nm}^*$, $II_\Omega^* = \Omega_{mn}^*\Omega_{nm}^*$, $IV^* = S_{mn}^*\Omega_{nk}^*\Omega_{km}^*$ as follows:

$$\beta_1 = -\frac{N}{Q}, \quad \beta_3 = -\frac{2IV^*}{NQ_1}, \quad \beta_4 = -\frac{1}{Q}, \quad \beta_6 = -\frac{N}{Q_1}, \tag{5}$$

where

$$Q = \left(N^2 - 2II_\Omega^*\right)/A_1, \quad Q_1 = Q\left(2N^2 - II_\Omega^*\right)/6, \quad N = C_1' + \frac{9}{4}\sqrt{2\beta^* II_S^*}. \tag{6}$$

The SST NL model [9] is a combination of the SST and S BSL EARSM models. Its expression for the Reynolds stresses τ_{ij} contains two terms: a linear term taken from the SST model (1), and a nonlinear term based on the S BSL EARSM model (2):

$$\tau_{ij} = \frac{2}{3}k\delta_{ij} - 2\nu_t S_{ij} + k\left(\beta_4 T_{4,ij} + \beta_6 T_{6,ij}\right). \tag{7}$$

Compared to the S BSL EARSM model, the nonlinear component has two simplifications: it does not use the term $T_{3,ij}$, and it uses the simplified expression $\tau = 1/(\beta^*\omega)$ as the turbulent time scale. The model constants appearing in (6) are $\beta^* = 0.09$, $A_1 = 1.8$, $C_1' = 1.8$.

The SST NL model is implemented in the TsAGI in-house CFD program Electronic Wind Tunnel (EWT-TsAGI [2]). In the presented simulations, a linearized implicit finite-volume scheme which is second-order in space and first-order in time is used for all equations. The convective fluxes are computed using the exact Godunov solution of the Riemann problem. Solution reconstruction in each cell is performed according to the MUSCL scheme. Diffusion fluxes are approximated by a modified second-order central difference scheme. The turbulence model source terms are computed using an unconditionally stable approximation analyzing the signs of the eigenvalues of the corresponding Jacobi matrix. More details on the numerical scheme, as well as validation results of EWT-TsAGI solver can be found in [3]. The code works with multi-block structured meshes and is parallelized using the MPI standard. All calculations discussed further in this paper have been performed using from 32 to 256 cores.

2. Test Cases

2.1. Flow in a Square Duct

A fully developed turbulent flow in a square duct is considered. The calculation of such a flow is a commonly used test for evaluating the ability of turbulence models to correctly describe the flow in corners, as it demonstrates the effect of turbulence anisotropy on the main flow, leading to significant changes in the flow structure. The width and height of the duct are 100 mm, the flow has the following parameters: density $\rho = 1.2\,\text{kg/m}^3$, pressure $p = 101325\,\text{Pa}$, temperature $T = 294.15\,\text{K}$, average velocity $U = 3\,\text{m/s}$. The Reynolds number, calculated from the average velocity and duct width, is $Re_b = 21400$. Simulation is performed for the duct length $L = 600$ mm with periodic boundary conditions that combine the inlet and outlet of the duct. To maintain a steady flow and compensate for the gas momentum losses caused by wall friction, a uniform pressure gradient is added by introducing an additional term into the equation system being solved. To compensate for the heating caused by friction, a constant wall temperature is set equal to the initial gas temperature $T_w = T = 294.15$ K. A structured grid containing 240 cells across the duct uniformly spaced ($y^+ \approx 1.25$) and 480 cells along the duct were used for the simulations. Due to symmetric formulation of the task, a quarter of the duct was simulated.

The calculations performed using the linear SST model, its non-linear modification SST NL and the DRSM model are compared with the results of the authors of the SST NL model [5] and DNS data [5, 16]. The differential Reynolds stress model used for the simulations was SSG/LRR-ω [4]. This model combines the Speziale–Sarkar–Gatski pressure-strain model in free

turbulent regions with the Launder–Reece–Rodi formulation near the wall by means of a blending function similar to that in SST model. The SSG/LRR-ω model was designed primarily for aerodynamic applications in the cases where anisotropic and three-dimensional effects are important.

The qualitative assessment of the simulation of secondary flows is performed by comparing the pattern of isolines of the longitudinal velocity profile in the duct cross section. Quantitative estimation is performed by comparing the longitudinal and transverse velocity profiles along the diagonal section of the duct. In Fig. 1 the numerical results of the considered flow using the SST and SST NL turbulence models are compared with the DNS results [5, 16]. The contours of the longitudinal velocity component and streamlines of a secondary flow are shown. It can be seen that the linear SST model significantly distorts the field of the longitudinal velocity component due to the absence of a secondary flow in the solution (see Fig. 1c). At the same time, the results obtained using the SST NL model predict the presence of a secondary flow and describe the longitudinal velocity field much better (Fig. 1b).

Figure 2 shows the distributions of the longitudinal and transverse velocity components along the diagonal of the duct cross section, which characterize the accuracy of the secondary flow intensity prediction. The figure compares EWT data (SST, SST NL, DRSM) with the results of the SST NL authors [5] and DNS data [16]. The graphs demonstrate that despite the relatively low values of the secondary flow velocity ($\sim 1\%$ of the average flow rate), it has a considerable influence on the flow structure. At the same time, the SST NL turbulence model provides a significant increase in the accuracy of the main flow calculation in comparison with the linear SST model. The difference of the longitudinal component of the flow velocity for the DNS and SST NL does not exceed 5% and this difference reaches 20% in the case of SST.

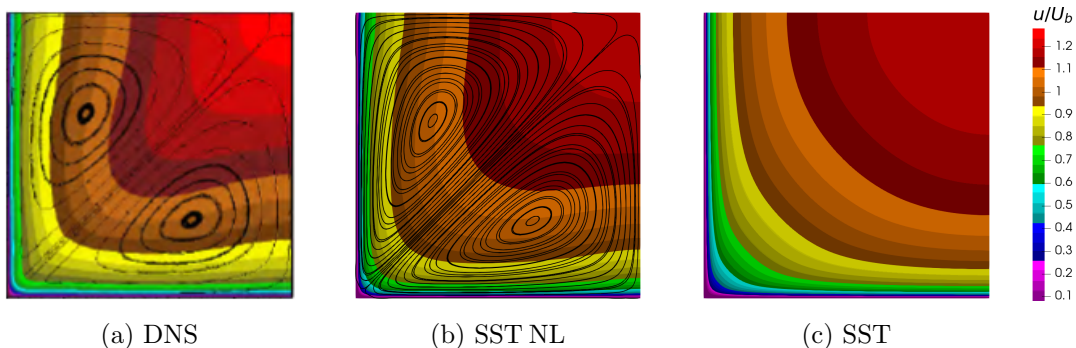(a) DNS   (b) SST NL   (c) SST

Figure 1. Comparison of longitudinal velocity distributions obtained using SST and SST NL turbulence models with DNS results [5]

2.2. Separated Flow in the Wing-body Junction

Validation of the SST NL turbulence model implementation was carried out by computing a separated flow at the NASA Juncture Flow model. This test confirms the ability of the tested turbulence model to correctly predict the presence of separation at the wing-body junction of an aircraft, as well as its dimensions. The model geometry and the experimental results are available on the official website [19]. In NASA experimental work, a detailed investigation of the flow around the model with a shortened DLR F6 wing (fuselage length of 4.84 m, wingspan of 3.4 m, see Fig. 3a) was performed to verify numerical methods within the Juncture Flow workshop. These experiments investigated separation generation at the wing-fuselage junction
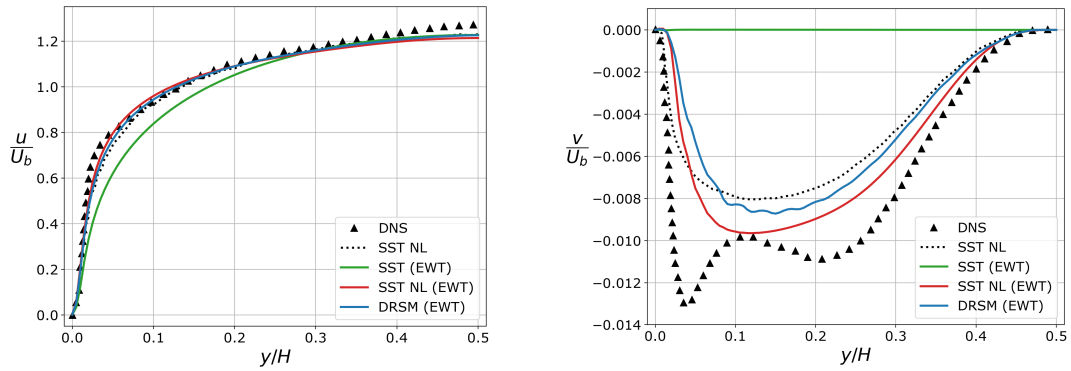
Figure 2. Distributions of the longitudinal and transverse velocity components along the diagonal of the duct cross section (DNS [16], SST NL [5], EWT)

and measured the longitudinal and transverse dimensions of the separation regions in various flow regimes, see Fig. 3b.

A multiblock structured grid with 85 million cells was used in calculations (Fig. 4). There were 324 cells per wing chord, boundary layer resolution was 64 cells, and the height of the first near-wall cell was $5 \cdot 10^{-6}$ m ($y^+ \approx 1.0$). Because of the symmetry of the problem, only half of the geometry was used. To estimate the errors associated with the discretization of the computational domain, the calculations were performed on a series of 3 grids generated from the base one by coarsening by a factor of 2 and 4 in each index direction. The following free flow parameters are considered: velocity $U = 64.4$ m/s, angle of the attack $\alpha = 5°$, pressure $p = 99000$ Pa, temperature $T = 288.84$ K. The quality of the corner flow simulation is assessed by comparing the numerical and experimental sizes of the separation region in the wing root.
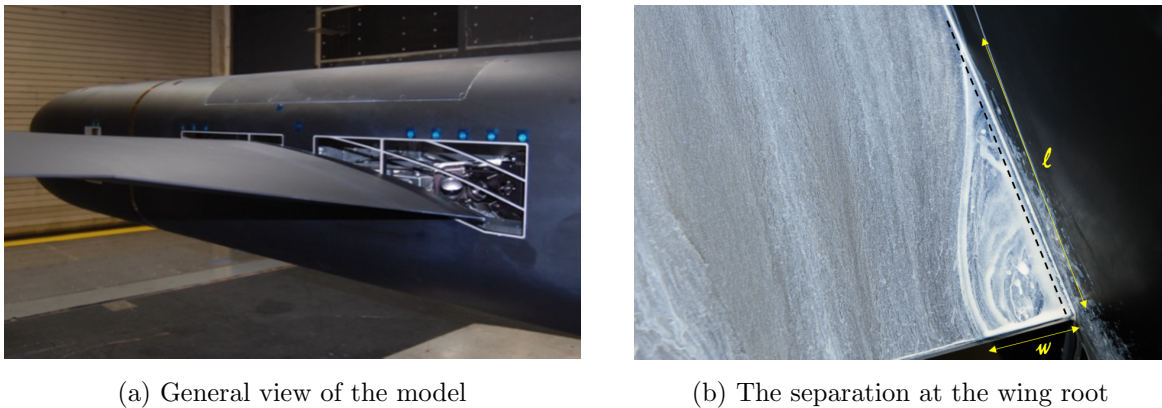

(a) General view of the model

(b) The separation at the wing root

Figure 3. NASA Juncture Flow test case [6]

Figure 5 shows the friction coefficient C_f distributions obtained with the linear and non-linear SST models. The linear version of the SST model predicts a developed diffuser separation at the wing-fuselage junction. In calculations with the SST NL turbulence model, the size of the separation region is much smaller compared to the SST.

Figure 6 shows the predicted separation sizes (length and width) as a function of $N^{-2/3}$, where N represents the number of grid cells. The power $-2/3$ refers to the second-order spatial accuracy: the results should vary linearly as the grid is refined ($N^{-2/3} \to 0$). The plots show that the solution predicted using the SST model depends on the grid resolution. The separation zone grows as the grid resolution increases, so on the finest grid, the separation size is significantly
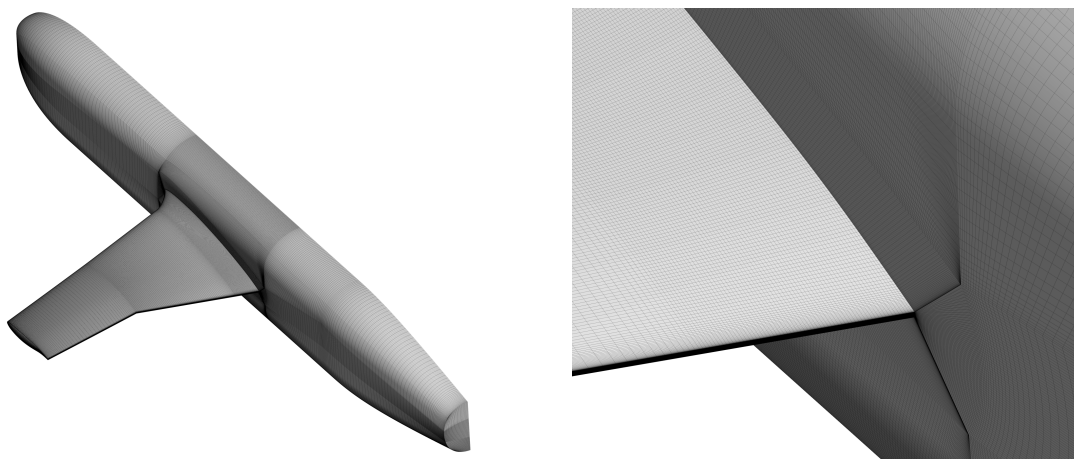
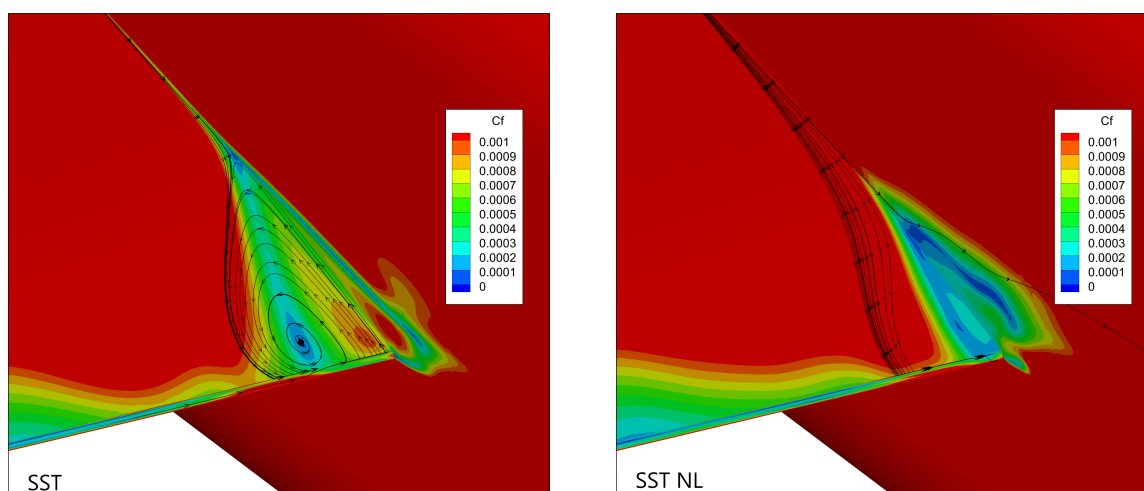**Figure 4.** The surface mesh of the Juncture Flow model

Figure 5. Distributions of the friction coefficient C_f obtained for the linear and nonlinear SST models

overestimated comparing to the experimental results [18]. The SST NL model, in general, permits to predict the longitudinal size of the separation zone more accurately: the discrepancy of numerical and experimental data is less than the experimental inaccuracy. However, the width of the separation zone in SST NL calculations with the finest grid is significantly underestimated. This fact requires additional computational investigations to study the influence of the grid resolution.

2.3. Transonic Wing Flow

Validation of the SST NL turbulence model at transonic flow regimes was performed on the well-known NASA Common Research Model (CRM). The model was developed for wind tunnel testing (NASA AMES 11-foot transonic wind tunnel, NASA National Transonic Facility). As a result, a database of experimental results has been obtained, that is used in CFD code validation benchmarks, such as AIAA Drag Prediction Workshop (DPW). The model geometry as well as the results of the experiments in different wind tunnels are available and can be found on the official website [17].
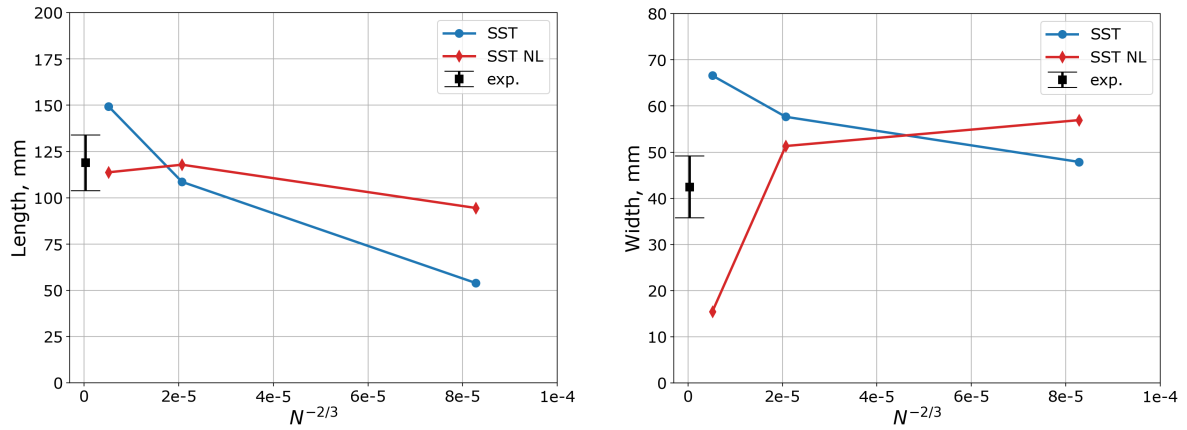
Figure 6. Predicted size of separation region at $\alpha = 5°$ on different grids (N is the number of grid cells) in comparison with experimental data [18]

The CRM model consists of a contemporary supercritical transonic wing and a fuselage that is representative of a widebody commercial transport aircraft. The model is designed for a cruise Mach number of $M_\infty = 0.85$ and a corresponding design lift coefficient $C_L = 0.5$. Leading edge sweep angle is $35°$, the wing reference area is $S = 0.280$ m^2, the wing span is $b = 1.5866$ m, and the mean aerodynamic chord is $c = 0.18914$ m.

The present study was performed using a series of multiblock structured computational grids prepared by the Royal Netherlands Aerospace Centre (NLR) as part of the AIAA 7th Drag Prediction Workshop. The provided grids take into account the aeroelastic deformations of the wing for each angle of attack. The geometries considered in this paper correspond to $\alpha = 2.5°$, $3°$, $3.5°$, and $4°$. The outer size of the computational domain was 150 m. The computational grid contains 1408 blocks, 36.3 million cells and correctly describes model geometry and flow around the model. There were 112 cells along the aircraft wingspan, 64 cells along the wing chord, 420 cells along the length of the fuselage (Fig. 7). In order to simulate the boundary layer correctly, 32 cells were placed in the near-wall layer of blocks, the dimensionless parameter of the first cell height near the solid surface y^+ did not exceed 1 for the whole model.
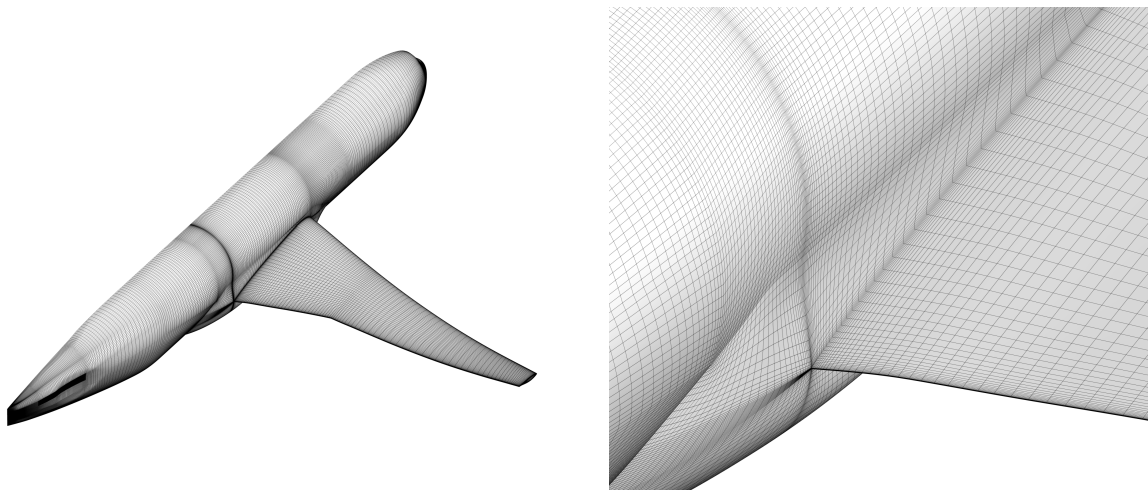

Figure 7. CRM surface grids

It is necessary to note the following observation made during work with the NLR series of grids. The linear dimensions of the model (wingspan, fuselage length, etc.), for which the grids were constructed, are smaller than the dimensions of the original CRM model by about 1.06 times. Therefore, all results presented in this paper were obtained on the grids scaled up by a factor of 1.06.

Numerical investigation was performed at the Reynolds number $\mathrm{Re}_c = 20 \cdot 10^6$ and Mach number M = 0.85. Six angles of attack were specified between 2.5° and 5.0° deg at 0.5° increments. For simulations with angles of attack $\alpha = 4.5°$ and 5°, mesh on deformed geometry for angle $\alpha = 4°$ was used. The results obtained with the original SST model and its non-linear modification SST NL are compared.

Figure 8 shows isentropic Mach number fields and streamlines on the upper wing surface at the angle of attack $\alpha = 5°$. It is evident that the obtained flow patterns differ significantly. The main difference is associated with the side of body (SOB) separation in the angular flow at the junction of the wing and fuselage. This separation appears in the SST calculations at $\alpha = 4°$ and grows as the angle of attack increases. In the results obtained using the SST NL model, SOB separation does not appear.

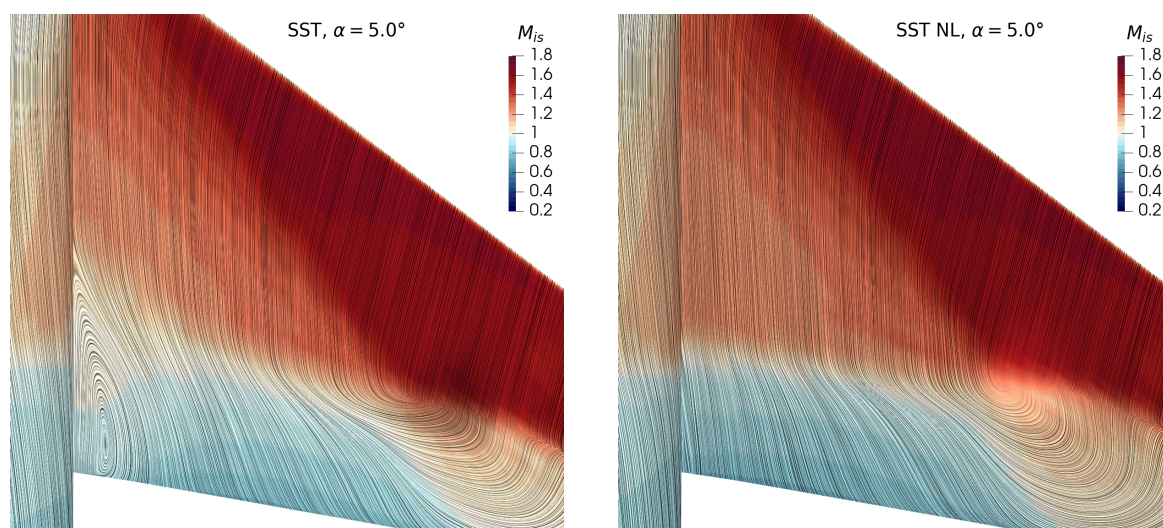**Figure 8.** Isoentropic Mach number and streamlines on the model surface, M = 0.85, $\alpha = 5.0°$

Another significant effect introduced by the nonlinear SST NL model is the upstream shift of the shock wave. Given at the Fig. 9 difference of the pressure coefficient values ($\Delta C_p = C_p^{\mathrm{nl}} - C_p^{\mathrm{sst}}$) illustrates the variations in the flow over the wing. At the angle of attack 3°, there is no SOB separation and the only difference in the flow is associated with a slight shift of the shock wave. As the angle of attack increases, the differences become more significant: in the SST solution SOB separation appears; in the SST NL solution shock wave shift increases. As a result, these differences lead to discrepancy in the aerodynamic characteristics, in particular, the lift coefficient C_L (Fig. 10). As can be seen in the figure, the discrepancy in the values of C_L is approximately 0.02.

Conclusion

The paper presents the results of simulation of anisotropic turbulent flows using the nonlinear model SST NL. Three tests are considered: flow in a square duct, corner flow separation at a
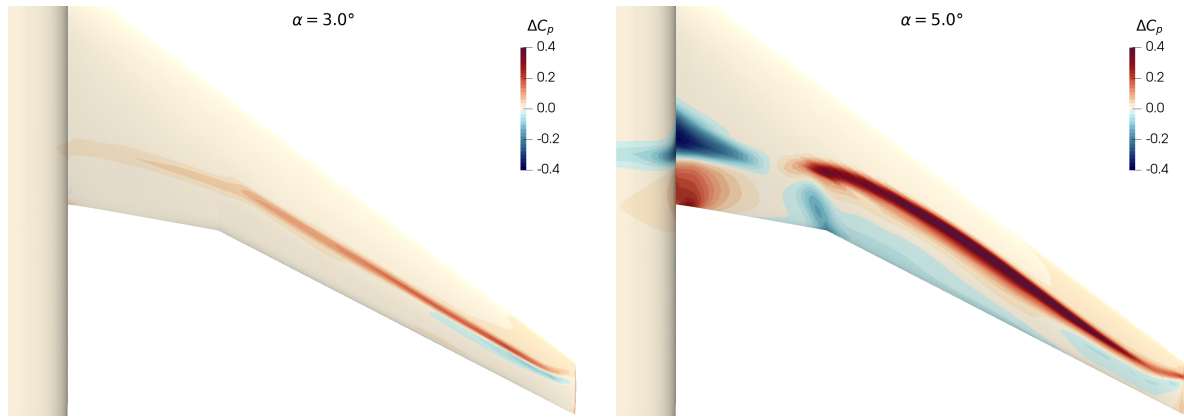
Figure 9. Difference in pressure coefficient values $\Delta C_p = C_p^{\mathrm{nl}} - C_p^{\mathrm{sst}}$, $\alpha = 3°$ and $5°$
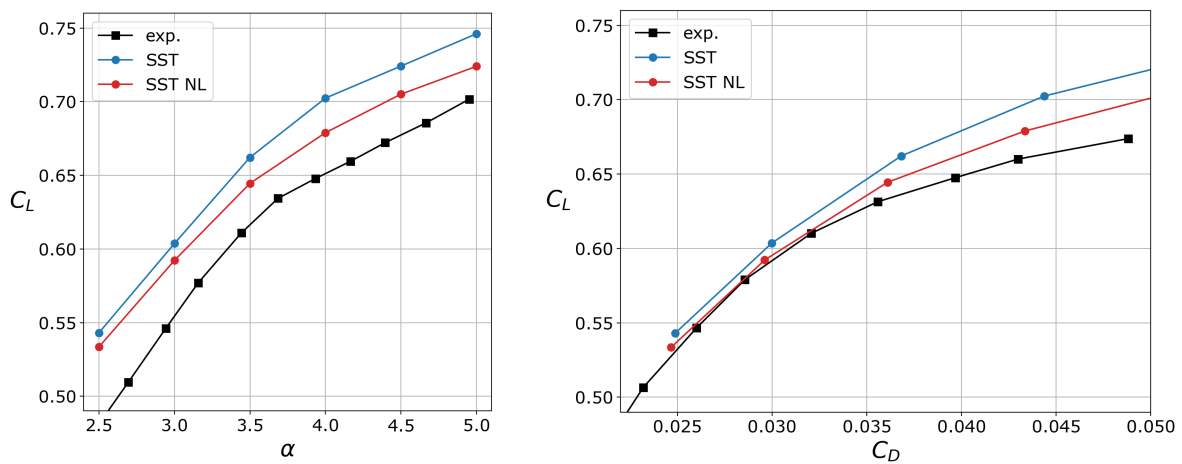

Figure 10. CRM wing-body lift and drag polar, $M = 0.85$, $\mathrm{Re} = 20 \cdot 10^6$
(experimental data [22])

wing-body junction, and transonic wing flow. The square duct flow calculations show that, in contrast to the linear SST, the SST NL model can simulate the secondary flow and therefore provides a significant increase in the accuracy of the main flow calculation. The test with juncture flow shows that the SST model tends to overestimate the separation size, which is typical for linear eddy viscosity models. On the contrary, the SST NL model correctly predicts the separation length, but underestimates its width. The results of the test with transonic wing flow do not allow drawing an unambiguous conclusion. On the one hand, the nonlinear model makes it possible to eliminate the false corner flow separation at the wing-body junction and thus to achieve a qualitative improvement in the simulation results. On the other hand, the nonlinear model predicts an upstream shifted location of the shock wave on the upper surface of the wing, which leads to underestimation of the lift force. This problem requires further investigation, possibly with a subsequent recalibration of the nonlinear term of the model.

Nevertheless, it can be concluded that the nonlinear model SST NL allows to significantly improve the quality of anisotropic flows simulation compared to linear SST model. Moreover, the SST NL model does not require a significant increase in computational cost as compared to the conventional SST. Tests have shown that the number of iterations required for convergence does not change, while the computation time of one iteration increases by 4–5 %.

Acknowledgements

References

1. Allmaras, S.R., Johnson, F.T., Spalart, P.R.: Modifications and clarifications for the implementation of the Spalart–Allmaras turbulence model. In: Seventh International Conference on Computational Fluid Dynamics (ICCFD7). pp. 1–11. No. 1902 (2012)

2. Bosnyakov, S., Kursakov, I., Lysenkov, A., *et al.*: Computational tools for supporting the testing of civil aircraft configurations in wind tunnels. Progress in Aerospace Sciences 44(2), 67–120 (2008). `https://doi.org/10.1016/j.paerosci.2007.10.003`

3. Bosnyakov, S.M., Gorbushin, A.R., Kursakov, I.A., *et al.*: About verification and validation of computational methods and codes on the basis of Godunov method. TsAGI Science Journal 48(7), 597–615 (2017). `https://doi.org/10.1615/TsAGISciJ.2018026173`

4. Cecora, R.D., Radespiel, R., Eisfeld, B., Probst, A.: Differential Reynolds-stress modeling for aeronautics. AIAA Journal 53(3), 739–755 (2015). `https://doi.org/10.2514/1.J053250`

5. Garbaruk, A.V.: Numerical simulation and stability analysis of wall-bounded turbulent flows. DSc Thesis, Peter the Great St. Petersburg Polytechnic University (2020)

6. Kegerise, M.A., Neuhart, D.H.: An experimental investigation of a wing-fuselage junction model in the NASA Langley 14- by 22-foot subsonic tunnel. NASA TM (220286), 1–195 (2019). `https://doi.org/10.2514/6.2019-0077`

7. Launder, B.E., Reece, G.J., Rodi, W.: Progress in the development of a Reynolds-stress turbulence closure. Journal of Fluid Mechanics 68(3), 537–566 (1975)

8. Matyash, E.S., Savelyev, A.A., Troshin, A.I., Ustinov, M.V.: Allowance for gas compressibility in the γ-model of the laminar-turbulent transition. Computational Mathematics and Mathematical Physics 59(10), 1720–1731 (2019). `https://doi.org/10.1134/S0965542519100117`

9. Matyushenko, A.A., Garbaruk, A.V.: Non-linear correction for the k-ω SST turbulence model. Journal of Physics: Conference Series 929(1), 1–6 (2017). `https://doi.org/10.1088/1742-6596/929/1/012102`

10. Menter, F.R., Garbaruk, A.V., Egorov, Y.: Explicit algebraic Reynolds stress models for anisotropic wall-bounded flows. Progress in Flight Physics 3, 89–104 (2012). `https://doi.org/10.1051/eucass/201203089`

11. Menter, F.R., Kuntz, M., Langtry, R.: Ten years of industrial experience with the SST turbulence model. Turbulence Heat and Mass Transfer 4, 625–632 (2003)

12. Menter, F.R.: Zonal two equation k-ω turbulence models for aerodynamic Flows. AIAA Paper (2906) (1993)

13. Morrison, J.H.: 7th AIAA CFD Drag Prediction Workshop. `https://aiaa-dpw.larc.nasa.gov`, accessed: 2022-09-10

14. Morrison, J.H., Kleb, B.: Observations on CFD verification and validation from the AIAA drag prediction workshops. AIAA Paper (0202), 1–21 (2014). `https://doi.org/10.2514/6.2014-0202`

15. Pope, S.: A more general effective-viscosity hypothesis. Journal of Fluid Mechanics 72, 331–340 (1975)

16. Raiesi, H., Piomelli, U., Pollard, A.: Evaluation of turbulence models using direct numerical and large-eddy simulation data. Journal of Fluids Engineering 133(2) (2011). `https://doi.org/10.1115/1.4003425`

17. Rivers, M.: NASA Common Research Model. `https://commonresearchmodel.larc.nasa.gov`, accessed: 2022-09-10

18. Rumsey, C.L., Lee, H.C., Pulliam, T.H.: Reynolds-averaged Navier–Stokes computations of the NASA Juncture Flow model using FUN3D and OVERFLOW. AIAA Paper (1304), 1–31 (2020). `https://doi.org/10.2514/6.2020-1304`

19. Rumsey, C.: NASA Juncture Flow. `https://turbmodels.larc.nasa.gov/Other_exp_Data/junctureflow_exp.html`, accessed: 2022-09-10

20. Spalart, P.R.: Strategies for turbulence modelling and simulations. International Journal of Heat and Fluid Flow 21(3), 252–263 (2000). `https://doi.org/10.1016/S0142-727X(00)00007-2`

21. Spalart, P.R., Allmaras, S.R.: A one-equation turbulence model for aerodynamic flows. AIAA Paper (0439) (1992). `https://doi.org/10.2514/6.1992-439`

22. Tinoco, E., Keye, S.: Drag predictions at and beyond cruise for the Common Research Model by an international collaborative community (2022)

23. Tinoco, E.N., Brodersen, O.P., Keye, S., *et al.*: Summary data from the sixth AIAA CFD drag prediction workshop: CRM cases. Journal of Aircraft 55(4), 1352–1379 (2018). `https://doi.org/10.2514/1.C034409`

24. Wallin, S., Johansson, A.V.: An explicit algebraic Reynolds stress model for incompressible and compressible turbulent flows. Journal of Fluid Mechanics 403, 89–132 (2000). `https://doi.org/10.1017/S0022112099007004`